Polylactide Degradation Activates Immune Cells by Metabolic Reprogramming

Chima V. Maduka[1,2,3], Mohammed Alhaj[4], Evran Ural[2,3], Michael O. Habeeb[2,3], Maxwell M. Kuhnert[2,3], Kylie Smith[2,3], Ashley V. Makela[2,3], Hunter Pope[2,3], Shoue Chen[5], Jeremy M. Hix[3], Christiane L. Mallett[3], Seock-Jin Chung[2,3], Maxwell Hakun[2,3], Anthony Tundo[2,3], Kurt R. Zinn[2,3], Kurt D. Hankenson[6], Stuart B. Goodman[7,8], Ramani Narayan[4], Christopher H. Contag[2,3,9]*

[1] Comparative Medicine & Integrative Biology, Michigan State University, East Lansing, MI 48824, USA
[2] Department of Biomedical Engineering, Michigan State University, East Lansing, MI 48824, USA
[3] Institute for Quantitative Health Science & Engineering, Michigan State University, East Lansing, MI 48824, USA
[4] Department of Chemical Engineering & Materials Science, Michigan State University, East Lansing, MI 48824, USA
[5] School of Packaging, Michigan State University, East Lansing, MI, 48824 USA
[6] Department of Orthopedic Surgery, University of Michigan Medical School, Ann Arbor, MI 48109, USA.
[7] Department of Orthopedic Surgery, Stanford University, CA 94063, USA.
[8] Department of Bioengineering, Stanford University, CA 94305, USA.
[9] Department of Microbiology & Molecular Genetics, Michigan State University, East Lansing, MI 48864, USA.

*Corresponding author: Christopher H. Contag, contagch@msu.edu

ABSTRACT

Polylactide (PLA) is the most widely utilized biopolymer in medicine. However, chronic inflammation and excessive fibrosis resulting from its degradation remain significant obstacles to extended clinical use. Immune cell activation has been correlated to the acidity of breakdown products, yet methods to neutralize the pH have not significantly reduced adverse responses. Using a bioenergetic model, we observed delayed cellular changes that were not apparent in the short-term. Amorphous and semi-crystalline PLA degradation products, including monomeric L-lactic acid, mechanistically remodel metabolism in cells leading to a reactive immune microenvironment characterized by elevated proinflammatory cytokines. Selective inhibition of metabolic reprogramming and altered bioenergetics both reduce these undesirable high cytokine levels and stimulate anti-inflammatory signals. Our results present a new biocompatibility paradigm by identifying metabolism as a target for immunomodulation to increase tolerance to biomaterials, ensuring safe clinical application of PLA-based implants for soft- and hard-tissue regeneration, and advancing nanomedicine and drug delivery.

Keywords: Polylactide, Metabolic Reprogramming, Immune Cells, Tissue Regeneration, Biocompatibility

Polylactide (PLA) is the most widely utilized biopolymer[1], with applications in nanotechnology, drug delivery and adult reconstructive surgery for tissue regeneration. However, after surgical implantation, PLA elicits adverse immune responses in up to 44% of human patients, often requiring further interventions[2,3]. In animals, a 66% incidence of excessive fibrosis with capsules from long-term inflammation which significantly limit implant-tissue integration has been reported[4]. PLA degrades by hydrolysis into D- or L-lactic acid, with semi-crystalline PLA degrading slower and tending to contain less D-content than amorphous PLA[1,5]. Adverse responses to PLA are exacerbated by mechanical loading and increasing implant size[6], and occur after prolonged exposure to large amounts of PLA degradation products[2,7-9]. It is speculated that adverse responses are mediated by PLA degradation reducing pH in surrounding tissue[10], the historical basis of which involved *Photobacterium phosphoreum*[11]. This bacterium expresses a luciferase whose reduced metabolic activity, measured by bioluminescence, can infer toxicity. In this study, breakdown products (extract) of PLA were obtained either in sterile water or Tris buffer; addition of acidic extract correlated with reduced luminescence. However, the study was not performed on mammalian cells, did not reflect the buffered in-vivo microenvironment or simulate prolonged exposure times to accumulated

54   PLA degradation products. Establishing that a decrease in pH correlates with PLA degradation has
55   informed the current strategy in regenerative medicine to neutralize acidic PLA degradation products both
56   in-vitro and in-vivo using polyphosphazene[12], calcium carbonate, sodium bicarbonate and calcium
57   hydroxyapatite salts[10], bioglass[13] and composites containing alloys or hydroxides of magnesium[14,15] despite
58   reports of failures[16]. The lack of a clearly described mechanism of immune cell activation by PLA
59   degradation remains a major obstacle in the safe application of large-PLA based implants in load-bearing
60   applications as reflected by their paucity in FDA approvals[17], and in soft tissue surgery where neutralizing
61   ceramics cannot be applied[18].
62   Metabolic reprogramming refers to significant changes in oxidative phosphorylation and glycolytic
63   flux patterns and is a driver of fibrosis and bacterial lipopolysaccharide (LPS)-induced inflammation[19,20].
64   Here we set out to establish a molecular mechanism that directly links metabolic reprogramming to
65   inflammation and fibrosis, consequent to cellular interactions with PLA degradation products. Foremost, we
66   develop and validate a bioenergetic model of prolonged immune cell interaction with accumulated PLA
67   degradation products. Only after prolonged exposure to amorphous or semi-crystalline PLA degradation
68   products did macrophages and fibroblasts mechanistically undergo metabolic reprogramming and marked
69   bioenergetic changes, with higher PLA crystallinity delaying onset. Using our model, we observed that PLA
70   breakdown products markedly increase proinflammatory cytokine expression in primary macrophages
71   through lactate signaling. Targeting different glycolytic steps using small molecule inhibitors modulated
72   proinflammatory and stimulated anti-inflammatory cytokine expression by inhibiting metabolic
73   reprogramming and altered bioenergetics in a dose-dependent manner. This process is highly specific and
74   not cytotoxic to surrounding unaffected immune cells. Further, we demonstrate that use of the small
75   molecule inhibitors imbedded in PLA implants substantiated our hypothesis of controlling the inflammatory
76   response in-vivo. Our findings establish a new biocompatibility paradigm by identifying altered metabolism
77   as a target for immunomodulation of PLA-based implants, fundamentally differing from previous strategies
78   aimed at neutralizing PLA. Therefore, major advances in the use of PLA for human and veterinary
79   applications are anticipated.
80
81   **Bioenergetic model for evaluating cellular responses to PLA degradation.**
82   To simulate in-vivo buffer conditions, breakdown products of PLA, generally referred to as
83   extracts[21], were generated in serum-containing DMEM medium and used after 12 days (d) of incubation in
84   a shaker at 37 °C (Fig. 1a). This in-vitro degradation method was designed to mimic PLA degradation in-
85   vivo, with agitation to accelerate PLA degradation relative to static methods[22]. Due to the buffering inherent
86   in the serum-containing DMEM medium, there were no changes in pH over the 12 d extraction period for
87   serum-containing control medium (pH = 8.0), amorphous PLA (pH = 8.2) and crystalline PLA (pH = 8.2)
88   extracts used on cells. On the other hand, extraction in water for the same duration resulted in pH
89   differences between control (pH = 8.2), amorphous PLA (pH = 7.5) and crystalline PLA (pH = 7.6) extracts.
90   Together, studies in rodents, dogs and humans indicate that adverse immune responses occur
91   after accumulation of PLA degradation products over several weeks or months[8,23-25]. To account for these
92   extended exposure times in our model, we cultured immune cells in PLA extract for 12 d, and this required
93   initiating our cultures with small numbers of cells per well in both control and treatment groups to prevent
94   overgrowth of the cultures. Mouse embryonic fibroblasts (NIH 3T3 cells) were stably transfected with a
95   Sleeping Beauty transposon plasmid (pLuBIG) having a bidirectional promoter driving a modified firefly
96   luciferase gene (fLuc) and a fusion gene encoding a Blasticidin-resistance marker (BsdR) linked to eGFP
97   (BGL)[26]. Seeding the same cell numbers across control and treatment groups resulted in constant levels of
98   luciferase and we exposed cells to equal levels of D-luciferin and oxygen in all assays. In this manner, ATP
99   was rate-limiting and changes in ATP were measured by bioluminescence using in-vivo imaging system
100 (IVIS; Fig. 1b). Use of bioluminescence as an indicator of ATP levels was inexpensive, rapid (on the order
101 of seconds) and allowed for high throughput temporal bioenergetic analysis in live cells. Additionally, in our
102 model, each well of a 96-well plate had a total of 200 μl of medium, of which 100 μl was freshly prepared.
103 The additional 100 μl for control wells was medium that had been in the shaker at 37 °C for 12 d to account
104 for potential nutrient degradation that could confound results. Similarly, the additional 100 μl for treatment
105 wells was medium in which PLA had been degraded under the same conditions.
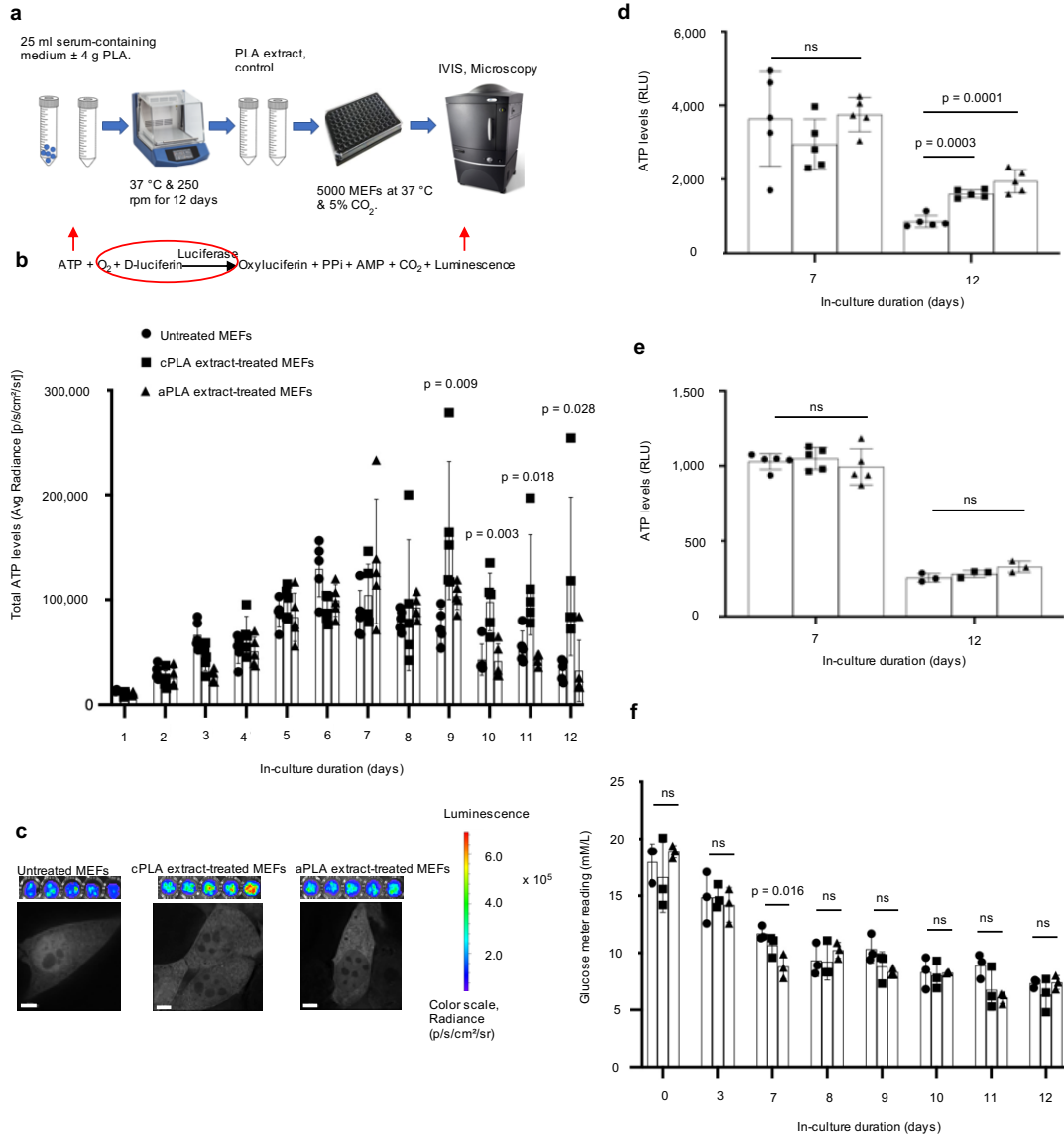
2

Figure 1 | Bioenergetic (ATP) levels are elevated in mouse embryonic fibroblasts (MEFs) only after prolonged exposure to polylactide (PLA) degradation products (extract). a, Workflow showing our in-vitro bioenergetic model. **b**, Keeping luciferase, oxygen and D-luciferin levels constant (red circle) allows for changes in ATP (red arrow) to be measured by luminescence (red arrow). Using in-vivo imaging system (IVIS) and in comparison to controls, ATP levels in live cells are increased in blasticidin-eGFP-luciferase (BGL)-transfected MEFs after prolonged exposure to crystalline PLA (cPLA) degradation products. **c**, Representative microscopic (scale bars, 5 μM) and IVIS images show differential nucleoli number and luminescence, respectively. **d**, Measuring ATP in cell lysates of wild-type MEFs revealed that prolonged exposure to both amorphous PLA (aPLA) and cPLA results in elevated ATP levels. **e**, Addition of PLA does not affect the biochemical reaction by which ATP is measured. **f**, Between groups on the same day, glucose levels are similar in our in-vitro bioenergetic model. Not significant (ns), mean (SD), n = 5 (Fig. 1b, 1d and day 7 for 1e) or n = 3 (Fig. 1f and day 12 for 1e), one-way ANOVA followed by Tukey's post-hoc test; 100 μl of control or PLA extract was used.

106
107
108   Dose-bioenergetic response of amorphous and crystalline PLA extracts revealed altered ATP levels for all
109   tested doses (Supplementary Fig. 1a). Therefore, we selected 100 or 150 μl of extract, as indicated in figure
110   legends, to mimic accumulation of voluminous PLA breakdown products[2,7].
111   Highly crystalline and amorphous PLA samples were selected for their high molecular weights and
112   represent a range of physicochemical properties (crystallinity, stereochemistry, degradation period) which
113   constitute important considerations in selecting PLA for hard and soft tissue engineering[8,10,25]. Before using
114   these PLA materials, we authenticated their physicochemical and thermal properties (Supplementary Table
115   1). Lastly, we used the non-transformed, immortalized NIH 3T3 fibroblast cell line that typifies primary

116 fibroblasts, as well as primary bone-marrow derived macrophages, both of which are key cellular mediators
117 of prolonged inflammation and excessive fibrosis that occur in response to PLA degradation[12,23].
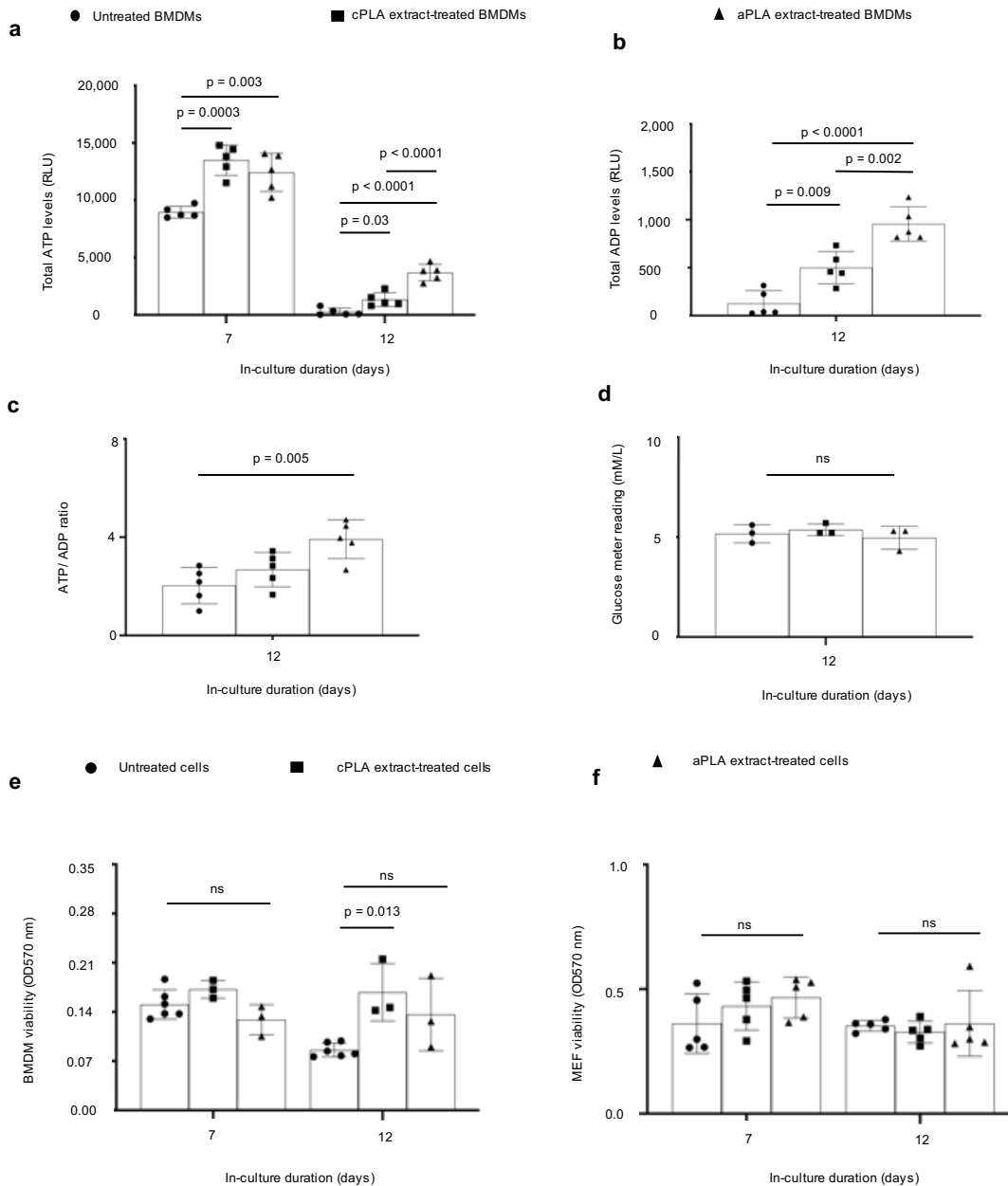118

Figure 2 | Bioenergetics is increased in primary bone marrow-derived macrophages (BMDMs) after prolonged exposure to polylactide (PLA) degradation products (extract). **a**, ATP levels **b**, ADP levels **c**, and ATP/ADP ratios are increased in BMDMs after prolonged exposure to amorphous PLA (aPLA) or crystalline PLA (cPLA) degradation products (extracts) in comparison to controls. **d**, Glucose levels between groups on day 12 are similar. **e-f**, Cell number between groups are similar for BMDMs (**e**) and MEFs (**f**). Not significant (ns), mean (SD), n = 5 (Fig. 2a, b, c, f), n = 3 (Fig. 2d), n = 3-6 (Fig. 2e), one-way ANOVA followed by Tukey's post-hoc test; 100 µl of control or PLA extract was used.

119
120 **Bioenergetics is altered in immune cells after exposure to PLA degradation products**
121   Unlike in the short-term (days 0-5), prolonged (days 6-12) exposure of fibroblasts to either
122 amorphous or crystalline PLA increased ATP levels in live cells (Fig. 1b-c). Upon high resolution z-stack
123 imaging, there were apparent changes in nucleoli number (Fig. 1c) after prolonged exposure to either
124 amorphous or crystalline PLA extract, which could represent a stress response[27]. To exclude the possibility
125 that changing luciferase expression (by transcription or translation) was responsible for observed

4

126　bioenergetic changes, we lysed wild-type cells after exposure to PLA extract and added controlled amounts
127　of luciferase and D-luciferin in the standard ATP assay. Moreover, measuring ATP levels in live cells by
128　IVIS is constrained by parameters inherent to live cells. Lysed cells allow for the measurement of ATP from
129　all organellar compartments, and is not constrained by D-luciferin uptake, revealing more information than
130　measurements in live cells. By day 12, there was a 1.9- and 2.3-fold increase in ATP levels among cells
131　exposed to crystalline and amorphous PLA extract, respectively (Fig. 1d). To exclude the possibility that
132　PLA extracts affect the biochemical reaction (Fig. 1b) underlying bioenergetic measurements, fibroblasts
133　were cultured for different time points. Thereafter, lysed fibroblasts were exposed to D-luciferin, luciferase
134　and control or PLA extract at the same time. No difference in ATP levels was observed, confirming that
135　treatment with PLA extract did not affect this biochemical reaction (Fig. 1e).
136　　　Declining ATP levels from day 0 to day 12 is likely due to changing glucose levels[28]. To determine
137　whether glucose levels changed between groups on the same day because of the extended exposure times
138　in our model, glucose meter readings were optimized in mammalian cell culture medium (Supplementary
139　Fig. 1b). Glucose levels were similar between groups on each day (Fig. 1f). On day 7, when untreated
140　groups had higher glucose levels (Fig. 1f), corresponding bioenergetic measurement revealed that PLA
141　extract-treated fibroblasts had higher ATP levels (Supplementary Fig. 1c), excluding changing glucose
142　levels as a confounding factor in our bioenergetic model. Because NIH 3T3 cells are normal immortalized
143　fibroblasts, changing cell number from proliferation could account for bioenergetic changes. To exclude
144　this, we optimized the crystal violet assay for cell number measurement[29] in fibroblasts (Supplementary Fig.
145　2a). Next, we isolated mouse primary bone marrow-derived macrophages (BMDMs) which, unlike NIH 3T3
146　cells, do not proliferate[30].
147　　　Both ATP[31] and ADP[32] metabolism and ratios are crucial in inflammatory conditions. In BMDMs
148　and consistent with our observations in fibroblasts, we observed marked increases in ATP and ADP levels
149　(Fig. 2a, b) or ATP/ADP ratios (Fig. 2c) which were not due to changing glucose levels (Fig. 2d). After
150　optimizing the crystal violet assay for macrophages (Supplementary Fig. 2b), overall, cell numbers could
151　not account for observed bioenergetic changes (Fig. 2e). Furthermore, fibroblast numbers were similar for
152　cultures that were untreated or exposed to PLA extracts (Fig. 2f), excluding changing cell number as a
153　confounder in our model.
154
155　**Exposure of macrophages to PLA breakdown products selectively results in metabolic**
156　**reprogramming**
157　　　To determine the metabolic pathways responsible for the bioenergetic changes we had observed,
158　Seahorse assays were used to measure oxygen consumption rate (OCR), extracellular acidification rate
159　(ECAR) and lactate-linked proton efflux rate (PER) in a customized medium (pH 7.4); this technique has
160　not been previously used to examine PLA-induced adverse responses. PLA extract was removed and
161　washed off the cells prior to running the Seahorse assay at a pH of 7.4. Seahorse assays measure ECAR
162　as an index of glycolytic flux, OCR as an index of oxidative phosphorylation and PER as an index of
163　monocarboxylate transporter function[33] in live cells; and are used to assess for metabolic reprogramming[34-
164　36]. Primary BMDMs exposed to amorphous PLA extract were metabolically altered, showing a 2-fold
165　increase in oxidative phosphorylation (OCR; Fig. 3a), 3.5-fold increase in glycolytic flux (ECAR; Fig. 3b)
166　and 3.5-fold increase in monocarboxylate transporter activity (PER; Fig. 3c) in comparison to untreated
167　BMDMs. Similar amounts (100 μl) of crystalline PLA extract resulted in a 1.6-fold increase in OCR (Fig. 3d)
168　but no change in ECAR (Fig. 3e) or PER (Fig. 3f). However, higher amounts (150 μl) of crystalline PLA
169　extract resulted in 3.2-, 3.8-, and 3.8-fold increases in OCR, ECAR and PER, respectively (Supplementary
170　Fig. 3a-c) compared to controls, suggesting that greater volume of PLA extract is required for
171　reprogramming using crystalline than amorphous PLA.
172　　　Next, we targeted different steps in the glycolytic pathway using three small molecule inhibitors: 3-
173　(3-pyridinyl)-1-(4-pyridinyl)-2-propen-1-one (3PO), 2-deoxyglucose (2DG) and aminooxyacetic acid (a.a.).
174　Whereas 3PO specifically inhibits 6- phosphofructo-2-kinase which is the rate limiting glycolytic enzyme[37],
175　2DG inhibits hexokinase, the first enzyme in glycolysis[36], and aminooxyacetic acid prevents uptake of
176　glycolytic substrates[38]. In a dose-dependent manner, 3PO, 2DG and a.a. inhibited metabolic
177　reprogramming following exposure to amorphous PLA (Fig. 3a-c) or crystalline PLA extract (Fig. 3-f), but
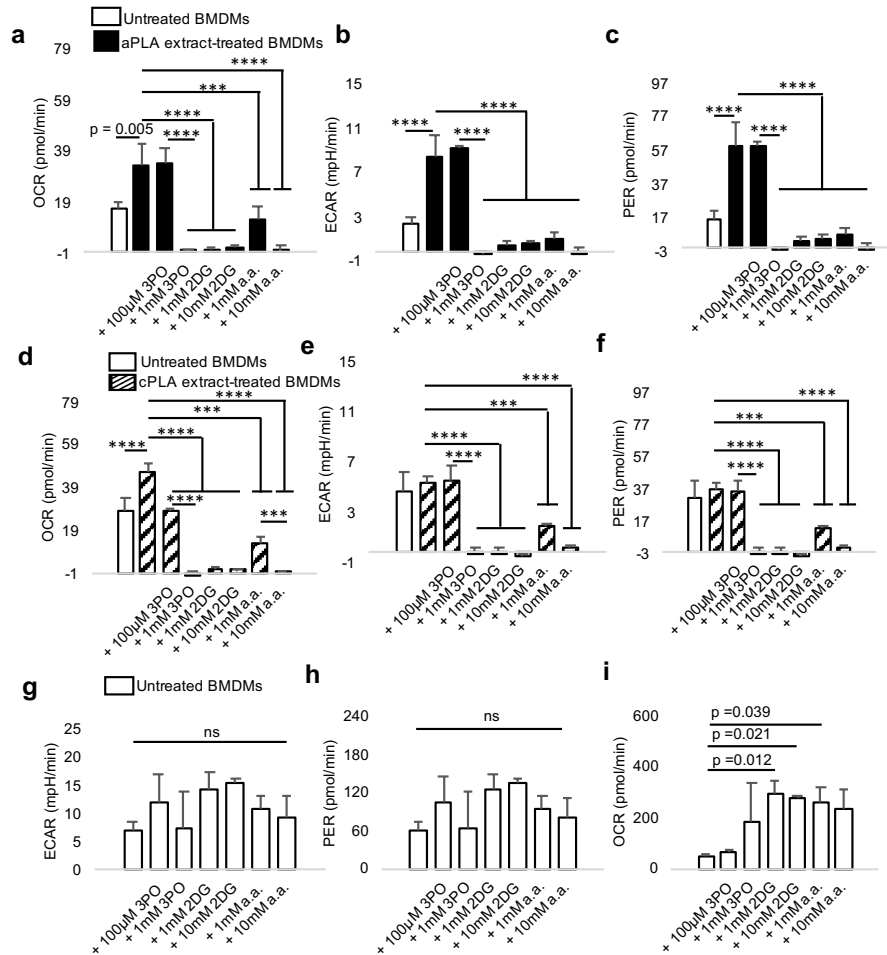178　not in untreated BMDMs (Fig. 3g-i).

Figure 3 | Functional metabolic indices are altered in primary bone marrow-derived macrophages (BMDMs) after prolonged exposure to polylactide (PLA) degradation products (extract), and can be modulated by glycolytic inhibitors. **a-c**, Following exposure to amorphous PLA (aPLA) extract, oxygen consumption rate (OCR) (**a**), extracellular acidification rate (ECAR) (**b**) and proton efflux rate (PER) (**c**) are increased relative to controls, and this abnormal increase can be dose-dependently controlled by various small molecule inhibitors. **d-f**, OCR (**d**) and not ECAR (**e**) and PER (**f**) are increased relative to controls in groups exposed to crystalline PLA (cPLA) extract, and functional metabolic indices can be controlled by pharmacologic inhibitors of glycolysis. **g-h**, ECAR (**g**) and PER (**h**) are not affected by glycolytic inhibitors in untreated BMDMs. **i**, Compensatory increase in OCR occurs in untreated BMDMs after treatment with some inhibitors. Not significant (ns), ***p<0.001, ****p<0.0001, mean (SD), n = 3, one-way ANOVA followed by Tukey's post-hoc test; 3-(3-pyridinyl)-1-(4-pyridinyl)-2-propen-1-one (3PO), 2-deoxyglucose (2DG) and aminooxyacetic acid (a.a.); 100 µl of control or PLA extract was used for 7 days.

179 This demonstrates cellular uptake of 3PO, 2DG and a.a., yet with selective pharmacologic effects. Notably
180 and under the same experimental conditions, cell viability was not reduced in untreated BMDMs after
181 exposure to glycolytic inhibitors (Supplementary Fig. 2c), demonstrating the absence of cytotoxicity[29].
182 However, when BMDMs were treated with amorphous or crystalline PLA extract, where metabolism was
183 abnormally remodeled, 3PO, 2DG and a.a. mildly, but selectively, reduced cell viability (Supplementary Fig.
184 2d). Therefore, pharmacologically targeting altered metabolism in primary BMDMs following exposure to
185 PLA extract is highly specific with limited toxicity to immune cells that have normal metabolic profiles.
186
187 **Fibroblasts are glycolytically reprogrammed after exposure to PLA breakdown products**
188   After prolonged exposure of fibroblasts to amorphous and crystalline PLA extracts, glycolytic flux
189 (ECAR; Fig. 4a-b) is increased by 1.6- and 1.7-fold, respectively. Furthermore, monocarboxylate transporter
190 function is increased in amorphous or crystalline PLA extract-treated fibroblasts by 1.6- and 1.5-fold,
191 respectively (Fig. 4c-d). However, oxidative phosphorylation remains similar between untreated fibroblasts
192 and cells exposed to amorphous or crystalline PLA extracts (OCR; Supplementary Fig. 4a-b). Remarkably,
193 increased bioenergetic (ATP) levels in amorphous or crystalline PLA extract-treated fibroblasts are inhibited
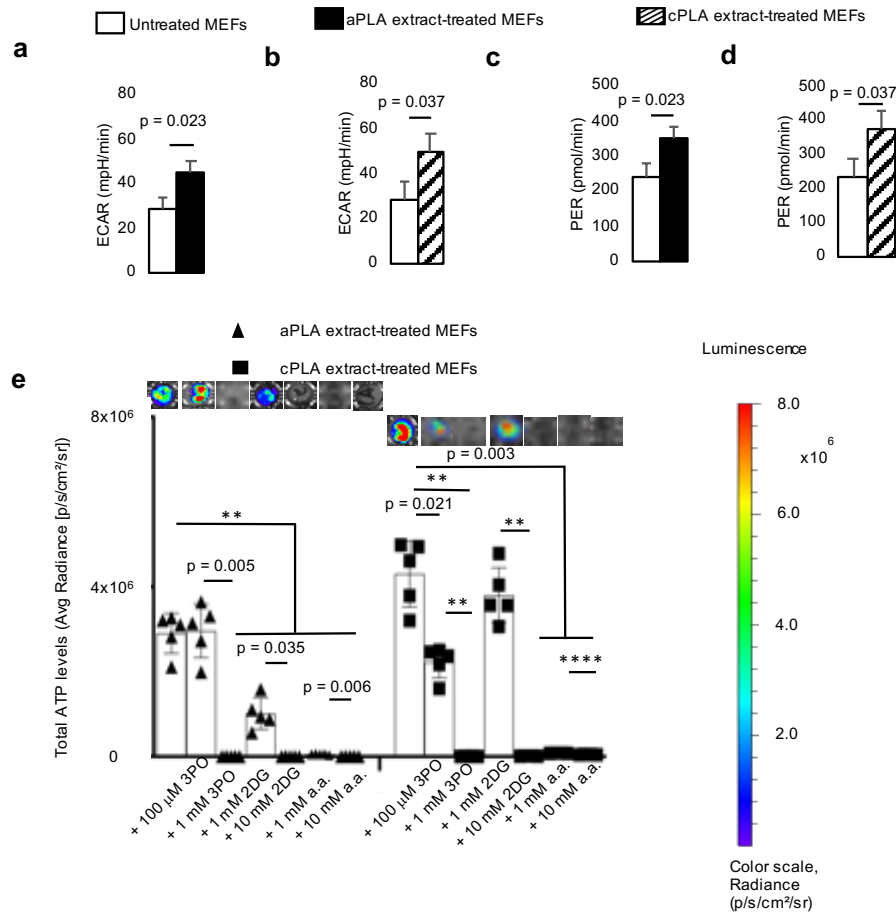194 by 3PO, 2DG and a.a. in a temporal and dose-dependent manner (Fig. 4e; Supplementary Fig. 4c).

Figure 4 | Functional metabolism is altered in mouse embryonic fibroblasts (MEFs) after exposure to polylactide (PLA) degradation products (extract). **a-b**, Following exposure to amorphous PLA (aPLA; **a**) or crystalline PLA (cPLA; **b**) extracts, extracellular acidification rate (ECAR) is increased. **c-d**, Proton efflux rate (PER) is elevated in MEFs after exposure to aPLA (**c**) or cPLA (**d**) extract. **e**, Bioenergetic levels in MEFs exposed to aPLA or cPLA extracts are decreased in a dose-dependent manner by 3-(3-pyridinyl)-1-(4-pyridinyl)-2-propen-1-one (3PO), 2-deoxyglucose (2DG) and aminooxyacetic acid (a.a.; representative wells are shown). ** $p = 0.002$, **** $p < 0.0001$, mean (SD), n = 3 (Fig. 4a, b, c, d), n = 5 (Fig. 4e), two-tailed unpaired t-test or Brown-Forsythe and Welch ANOVA followed by Dunnett's T3 multiple comparisons test; 100 µl of control or PLA extract was used for 7 days.

195
196 **Short- and long-term exposure to L-lactic acid alters bioenergetics and results in metabolic**
197 **reprogramming**
198 As previously reported for short-term hydrolytic degradation of PLA[8], there was no reduction in
199 mass of PLA after our 12 d extraction, but there were detectable changes in molecular weight
200 (Supplementary Table 2). Using the standard D/L-lactic acid enzyme-based determination assays could
201 not effectively measure levels in serum-containing medium. However, in milliQ water and relative to
202 controls, we observed a 7.8- and 5.2-fold increase in L-lactic acid in amorphous and crystalline PLA
203 extracts, respectively, although these increments were not significant (Supplementary Table 3;
204 Supplementary Fig. 5a-b). Similarly, we observed a 2.7- and 2.8-fold increase in D-lactic acid in amorphous
205 and crystalline PLA extracts, respectively (Supplementary Table 3). Therefore, we exposed BMDMs to
206 various doses of L-lactic acid, ranging from 2.5- to 15-fold higher levels in comparison to untreated cells. In

207 addition, we measured corresponding pH levels: Untreated medium (pH = 8.01), 2.5 mM (pH = 7.47), 5 mM
208 (pH = 7.19), 10mM (pH = 6.84) and 15mM (pH = 6.65) L-lactic acid-containing DMEM medium.
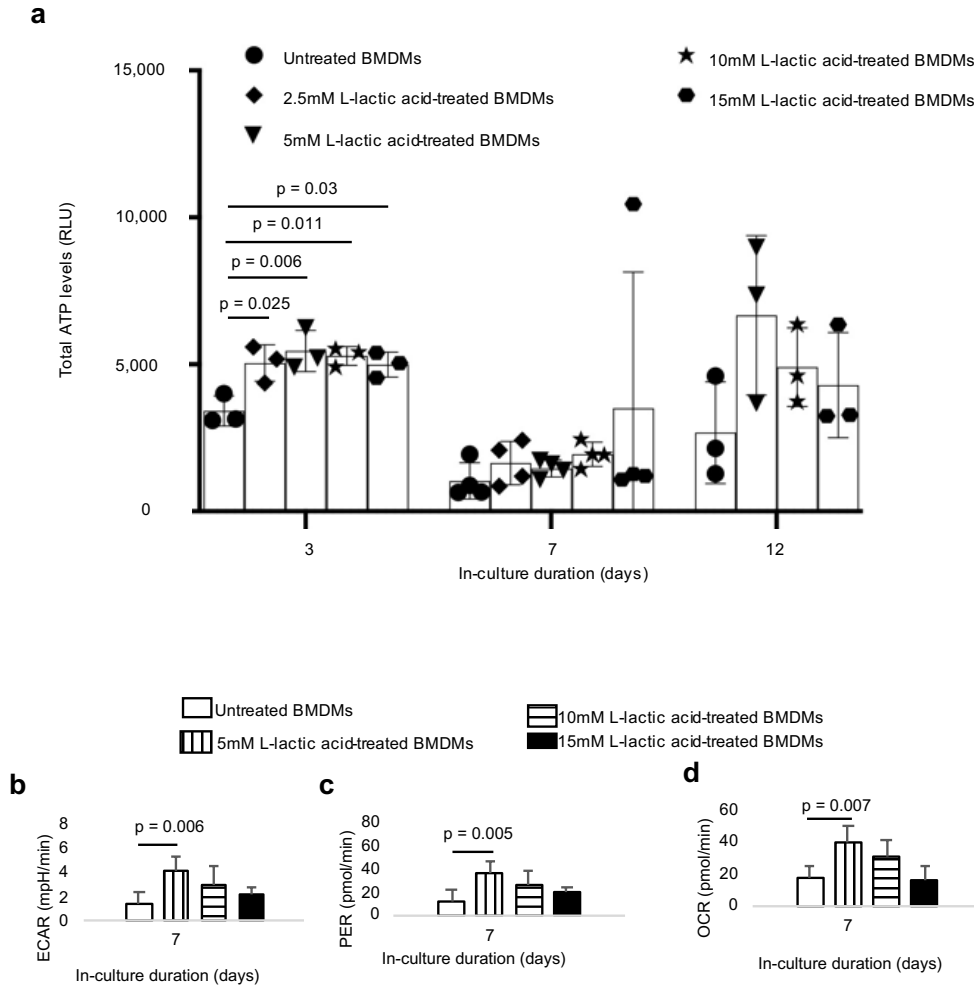

Figure 5 | Treatment of primary bone marrow-derived macrophages (BMDMs) with L-lactic acid altered bioenergetic (ATP) levels and functional metabolism. a, Treatment with different doses of monomeric L-lactic acid resulted in changes in ATP levels. **b-d**, Following exposure to L-lactic acid extracellular acidification rate (ECAR, **b**), proton efflux rate (PER, **c**) and oxygen consumption rate (OCR, **d**) are increased. One-way ANOVA followed by Tukey's post-hoc test, mean (SD), n = 3-4 (Fig. 5a), n = 5 (Fig. 5b, c, d).

209
210 We observed that bioenergetic levels are altered in the short-term (day 3; Fig. 5a) for all doses of
211 L-lactic acid treatment, resulting in a 1.5 to 1.6-fold increase in ATP levels. After prolonged (day 7) exposure
212 to L-lactic acid and even when bioenergetic alterations were not apparent, glycolytic flux (ECAR; Fig. 5b),
213 monocarboxylate transporter function (PER; Fig. 5c) and oxidative phosphorylation (OCR; Fig. 5d) were
214 increased by 2.8-, 2.8- and 2.3-fold, mechanistically reproducing observations made with amorphous and
215 crystalline PLA extracts in our bioenergetic model. Moreover, these changes were not dependent on
216 alterations in cell number (Supplementary Fig. 5c). Of note, highly acidic groups (10-15 mM L-lactic acid)
217 did not result in reduction in viability of primary macrophages either at day 7 or 12, relative to controls
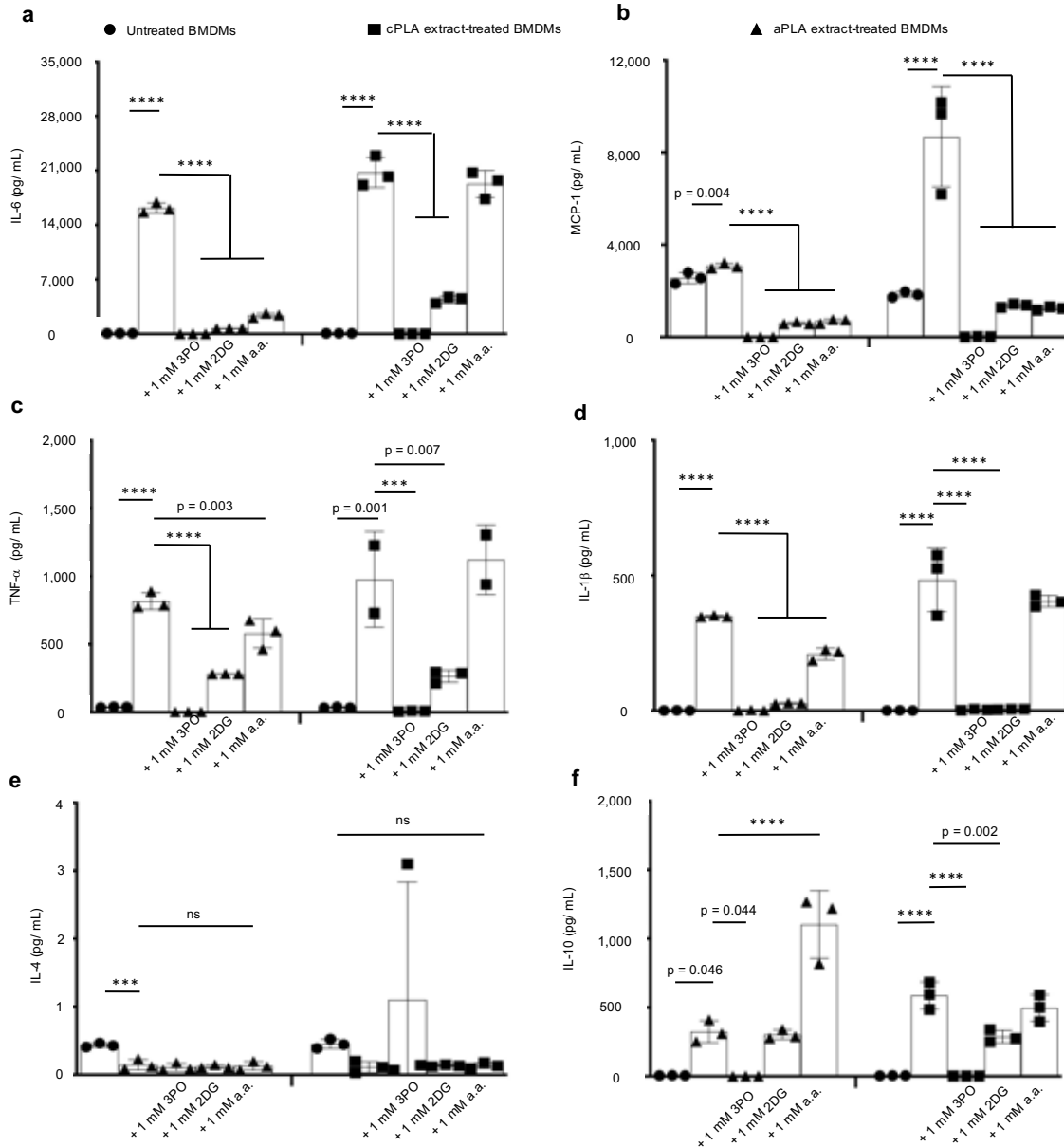218 (Supplementary Fig. 5c).
219
220
221

8

Figure 6 | In macrophages exposed to PLA breakdown products, glycolytic inhibitors modulate elevated proinflammatory cytokine expression and stimulate or do not reduce anti-inflammatory cytokine levels. **a-d**, Following exposure to amorphous PLA (aPLA) or crystalline PLA (cPLA) extract, primary bone marrow-derived macrophages (BMDMs) express elevated levels of IL-6 (**a**), MCP-1 (**b**), TNF-α (**c**) and IL-1β (**d**) in comparison to untreated BMDMs, and these elevated proinflammatory cytokine levels can be modulated by various small molecule inhibitors of glycolysis. **e**, Addition of glycolytic inhibitors to PLA does not reduce IL-4 expression. **f**, Expression of IL-10 is increased by inhibiting glycolysis using aminooxyacetic acid (a.a.) in amorphous PLA. Not significant (ns), ***p<0.001, ****p<0.0001, mean (SD), n = 3 in all except the cPLA group in TNF-α (Fig. 6c) where n=2-3, one-way ANOVA followed by Tukey's post-hoc test; 3-(3-pyridinyl)-1-(4-pyridinyl)-2-propen-1-one (3PO), 2-deoxyglucose (2DG); 100 µl of aPLA or 150 µl of cPLA extract with corresponding controls were used on day 7.

Glycolytic inhibition modulates proinflammatory and stimulates anti-inflammatory cytokine expression

To determine whether glycolytic inhibition affects proinflammatory (IL-6, MCP-1, TNF-α, IL-1β and IFN-λ) and anti-inflammatory (IL-4, IL-10, and 1L-13) protein expression, we used a magnetic bead-based chemokine and cytokine assay[39]. We observed that prolonged exposure of primary macrophages to amorphous and crystalline PLA extracts resulted in 228- and 319-fold increases, respectively, in IL-6 protein expression (Fig. 6a) compared to untreated macrophages. We confirmed this observation by ELISA

9

229　(Supplementary Fig. 6a). Similarly, exposure of macrophages to lactic acid resulted in elevated IL-6 protein
230　expression by 2.3-fold (Supplementary Fig. 6a). Amorphous PLA extracts increased MCP-1 (Fig. 6b), TNF-
231　α (Fig. 6c) and IL-1β (Fig 6d) levels by 1.2-fold, 21-fold, and 567-fold, respectively. Likewise, crystalline
232　PLA extracts increased MCP-1 (Fig. 6b), TNF-α (Fig. 6c) and IL-1β (Fig 6d) levels by 4.7-fold, 27-fold, and
233　1,378-fold, respectively. Abnormally increased levels of IL-6, MCP-1, TNF-α and IL-1β were modulated by
234　addition of 3PO, 2DG or a.a. (Fig. 6a-d). Increased MCP-1 levels in macrophages also occurred after
235　exposure to L-lactic acid (Supplementary Fig. 6b). Levels of IFN-γ and IL-13 were unchanged by PLA
236　extract (data not shown) but exposure to amorphous PLA extract decreased IL-4 protein levels by 3-fold
237　(Fig. 6e) relative to untreated macrophages. Remarkably, with the exception of 3PO, IL-10 expression was
238　either unchanged (crystalline PLA) or increased by 3.4-fold (amorphous PLA) upon addition of a.a. (Fig. 6f)
239　relative to macrophages exposed to PLA extract.
240
241　**Increased radiolabeled glucose uptake occurs in the PLA microenvironment and drives**
242　**inflammation, in-vivo**
243　　　　Taken together, our in-vitro data suggest that metabolic changes drive inflammation arising from
244　PLA degradation. To test this hypothesis in-vivo, we incorporated 2DG into amorphous PLA (aPLA) by
245　melt-blending at 190 °C and compared to aPLA which had been subjected to similar melt-blending
246　conditions (called reprocessed aPLA). Following melt-blending, extruded (sterile) filaments (1.75 mm
247　diameter, 1 mm long) were subcutaneously implanted on the back (dorsum) of mice. Sham controls
248　underwent similar surgical exposures but were not implanted with any materials. After 6 weeks, mice were
249　injected with F-18 fluorodeoxyglucose (FDG) and euthanized; using FDG allows for evaluation of metabolic
250　reprogramming and inflammation[40,41]. Thereafter, circular biopsies (12 mm in diameter) of full thickness
251　skin containing implants were assayed for radioactivity using a gamma counter. Compared to sham
252　controls, skin containing reprocessed aPLA implants had 1.35-fold increase in FDG uptake, which was
253　abolished in skin containing aPLA+2DG implants (Fig. 7a).
254　　　　Next, we sought to determine the effect of glycolytic inhibition on recruitment and activation states
255　of macrophages and fibroblasts. To compare the effects of glycolytic inhibition to neutralization techniques,
256　we included a group where hydroxyapatite (HA) was incorporated in aPLA[10,42]. Hematoxytin and eosin
257　staining revealed the presence of inflammatory infiltrates in the implant microenvironment (reprocessed
258　aPLA, aPLA+2DG, aPLA+HA) compared to sham controls, suggesting persistent inflammation
259　(Supplementary Fig. 7).
260　　　　Chronic inflammation to PLA is principally driven by recruited macrophages[12,23]. Therefore, we
261　stained for CD11b and F4/80, established macrophage markers. Compared to sham controls, aPLA
262　resulted in a 1.7- and 2.2-fold increase in CD11b and F4/80 intensities, respectively (Fig. 7b-c;
263　Supplementary Fig. 8). Unlike aPLA+2DG, aPLA+HA increased CD11b and F4/80 intensities by 2.6-fold
264　and 2.2-fold, respectively, when compared to sham controls (Fig. 7b-c). Of note, there was no significant
265　difference in CD11b and F4/80 intensities between aPLA and aPLA+2DG (Fig. 7b-c), suggesting similar
266　levels of macrophage recruitment. Furthermore, aPLA+2DG revealed 2.3-fold and 1.7-fold less CD11b and
267　F4/80 intensities, respectively, compared to aPLA+HA (Fig. 7b-c). To determine the activation states of
268　recruited macrophages, we stained for CD206 and CD86, anti-inflammatory and proinflammatory
269　macrophage markers, respectively[43]. Relative to other groups, only aPLA+HA increased CD206 intensity
270　(Fig. 7d; Supplementary Fig. 8), consistent with the bioactivity of HA[44]. We observed a 1.8-fold increase in
271　CD86 intensity with reprocessed aPLA compared to sham controls, consistent with the proinflammatory
272　effects of aPLA (Fig. 7e; Supplementary Fig. 8). Compared to reprocessed aPLA, aPLA+2DG and not
273　aPLA+HA decreased CD86 intensity (Fig. 7e). In fact, there was a 1.4-fold decrease in CD86 intensity in
274　aPLA+2DG compared to aPLA+HA (Fig. 7e).
275　　　　Fibroblasts are a key cellular player of excessive fibrosis around PLA implants[12,23], and their
276　activation in myofibroblast phenotype is marked by α-SMA and TGF-β expression[45]. We observed a 1.4-
277　fold increase in α-SMA intensity with reprocessed PLA compared to sham controls, which was decreased
278　in the aPLA+2DG, but not aPLA+HA group (Fig. 8a; supplementary Fig. Supplementary Fig. 9). With TGF-
279　β intensity, aPLA+HA was elevated relative to other groups (Fig. 8b; Supplementary Fig. 9). Compared to
280　aPLA+HA, aPLA+2DG revealed 1.4-fold and 1.8-fold decrease in α-SMA and TGF-β intensities,
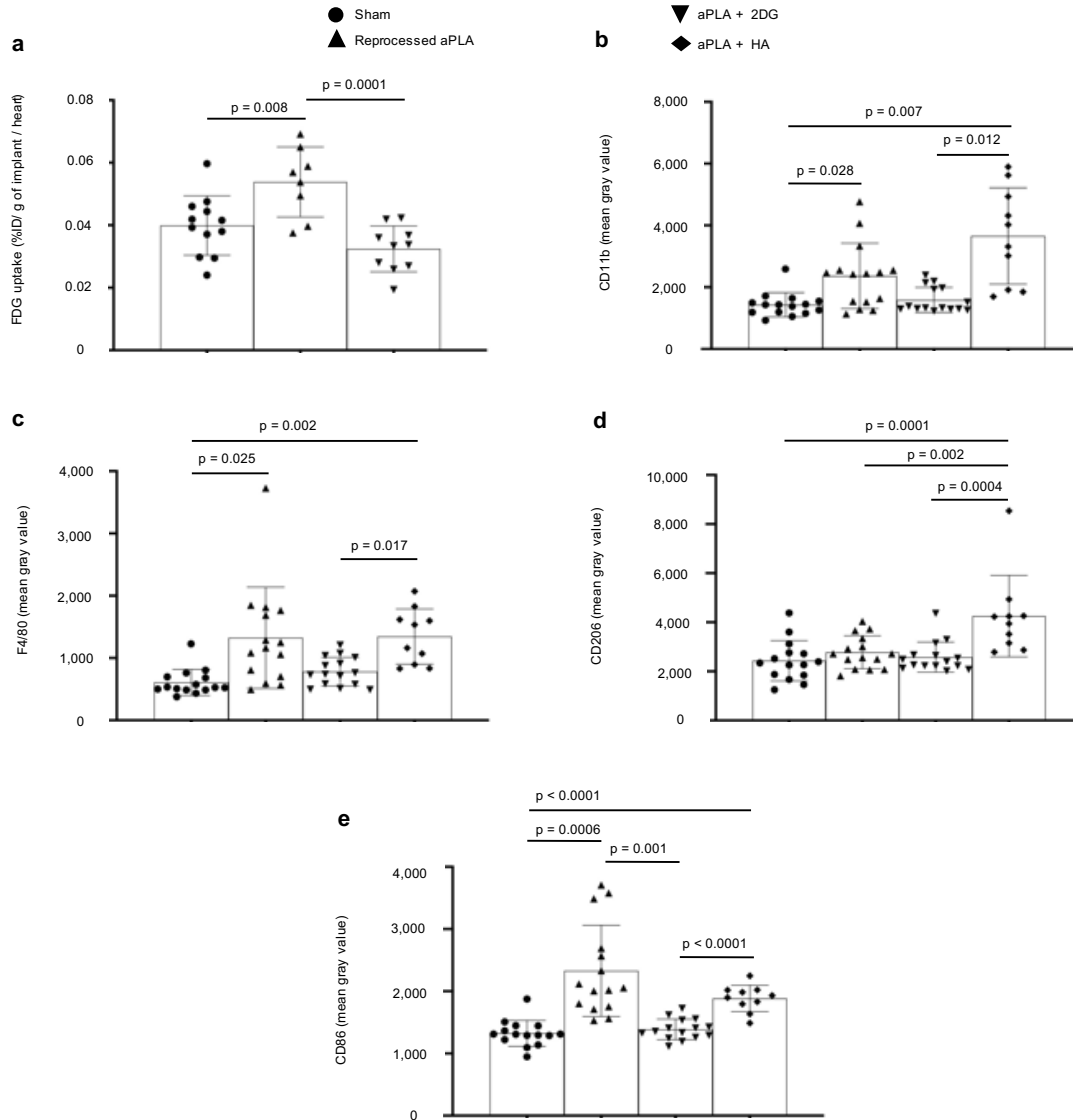281　respectively (Fig. 8b).

10

Figure 7 | Increased radiolabeled glucose uptake occurs in the polylactide (PLA) microenvironment and drives inflammation in-vivo. **a**, When normalized to heart values, percent injected dose per gram (% ID/ g) of biopsied tissues surrounding amorphous PLA (aPLA) implants show higher F-18 fluorodeoxyglucose (FDG) uptake compared to sham controls; increased FDG uptake is reduced by incorporation of 2-deoxyglucose (2DG). **b-c**, Compared to sham controls, mean fluorescence intensity of CD11b (**b**) or F4/80 (**c**) is increased following surgical implantation of aPLA or a combination of aPLA and hydroxyapatite (HA), but not a combination of aPLA and 2DG. **d**, Compared to other groups, CD206 mean fluorescence intensity is increased in aPLA + HA. **e**, Compared to sham controls, CD86 mean fluorescence intensity is increased following implantation of aPLA; elevated CD86 is decreased by incorporating 2DG but not HA. Mean (SD); Fig. 1a, sham (n = 12), aPLA (n = 8), aPLA + 2DG (n = 10); Fig 1b-e, sham (n = 15), aPLA (n = 15), aPLA + 2DG (n = 15), aPLA + HA (n = 10); one-way ANOVA followed by Tukey's post-hoc test or Brown-Forsythe and Welch ANOVA followed by Dunnett's T3 multiple comparison test; refer to methods section (In-vivo studies, tissue processing and analyses) for more information on n.
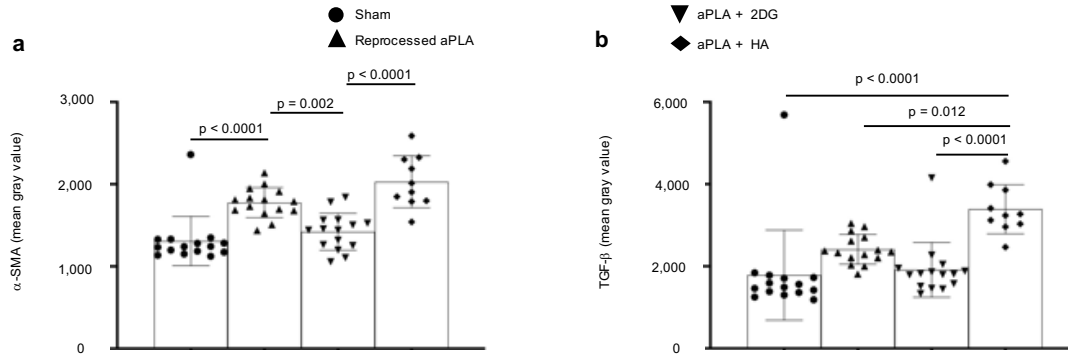
282
283

11

Figure 8 | Activation of fibroblasts in the polylactide (PLA) microenvironment is regulated by immunometabolism. **a**, Compared to sham controls, mean fluorescence intensity of alpha-smooth muscle actin (α-SMA) is increased following surgical implantation of amorphous PLA (aPLA) or a combination of aPLA and hydroxyapatite (HA), but not a combination of aPLA and 2-deoxyglucose (2DG). **b**, Compared to other groups, mean fluorescence intensity of transforming growth factor-beta (TGF-β) is increased in aPLA + HA. Mean (SD); sham (n = 15), aPLA (n = 15), aPLA + 2DG (n = 15), aPLA + HA (n = 10); one-way ANOVA followed by Tukey's post-hoc test; refer to methods section (In-vivo studies, tissue processing and analyses) for more information on n.

284

285 **Discussion**

286   We describe a bioenergetic model of immune cell activation to PLA degradation, revealing that
287 altered bioenergetics and metabolic reprogramming underlie adverse responses, including persistent
288 inflammation and excessive fibrosis, to PLA breakdown products. For decades, the hypothesis in
289 regenerative medicine has been that acidity drives immune cell activation to PLA degradation[10]. However,
290 this observation was founded on correlation and not causation[11,21]. Consequently, methods based on
291 neutralizing acidity have been inadequate in controlling adverse responses to PLA degradation[7,16].

292   Importantly, our in-vitro model extends the short time periods that have been previously studied[46].
293 By adapting our bioenergetic model for high throughput analysis, we observed delayed immune cell
294 changes not apparent in the short-term. In patients, PLA slowly degrades into oligomers and monomers of
295 lactic acid. Ultimately, due to bulk degradation, PLA breakdown exceeds immune cellular clearance,
296 resulting in accumulation of oligomers and monomers of lactic acid[25]. We illustrate that only after prolonged
297 exposure to PLA degradation products do fibroblasts and macrophages become activated. Mechanistically,
298 PLA degradation not only alters bioenergetic homeostasis in immune cells, it results in metabolic
299 reprogramming. We identified PLA degradation products to include monomeric L-lactic acid and reproduced
300 bioenergetic alterations and metabolic reprogramming using monomeric L-lactic acid. Although not shown,
301 we also identified a spectrum of different oligomeric lactic acid in extracts by electrospray ionization-mass
302 spectrometry as previously reported[47]. Following prolonged exposure of macrophages to PLA degradation
303 products, metabolic reprogramming is characterized by concomitantly elevated oxidative phosphorylation
304 and glycolysis, resulting in increased IL-6, MCP-1, TNF-α and IL-1β protein expression, potent
305 proinflammatory cytokines. Increased glycolysis, a fundamental proinflammatory metabolic phenotype, is
306 likely mediated by HIF-1α[36]. Human fibroblasts in lactate-enriched medium stabilize HIF-1α resulting in
307 increased glycolysis[48] which underlies activation of fibroblasts in several profibrotic pathologies[19]. Similarly,
308 increased oxidative phosphorylation is required for macrophages to function as antigen presenting cells as
309 part of inflammation[49] or its resolution[20].

310   Inhibiting different steps in the glycolytic pathway produced similar effects, decreasing
311 proinflammatory cytokine expression by modulating metabolic reprogramming and altered bioenergetics.
312 Unlike bacterial LPS-mediated glycolytic reprogramming that is uniquely dependent on IL-1β[36], PLA
313 degradation products additionally affect IL-6, MCP-1 and TNF-α. Of note, modulating proinflammatory
314 cytokine expression using aminooxyacetic acid stimulated IL-10 protein expression, an anti-inflammatory
315 cytokine[34]. Collectively, these findings are important for at least four reasons. First, it explains the
316 "Oppenheimer phenomenon", where long-term PLA implantation results in neoplasia in some humans and
317 up to 80% of rodents[6] since IL-6 directly links persistent inflammation from PLA to cellular transformation[50].
318 Second, stimulating IL-10 is critical to tissue repair by driving wound resolution and angiogenesis[51]. In fact,
319 IL-10 is a key immunomodulatory cytokine secreted by mesenchymal stem cells[52], and is crucial in
320 macrophage-stem cell crosstalk[53,54] for tissue engineering. Third, macrophages that have normal

12

321 metabolism are unaffected by the small molecule inhibitors studied. In fact, cytotoxicity is selective for
322 macrophages having altered metabolism, following exposure to PLA degradation products, making this
323 technique particularly desirable. Fourth, it provides a basis to study lactate signaling in tumor initiation, with
324 the potential to stop neoplastic initiation.
325 In cell culture medium used in our studies, serum and high bicarbonate salts buffered the pH of
326 PLA degradation products, excluding pH as a confounder of observed metabolic cellular changes.
327 Furthermore, using monomeric L-lactic acid at various concentrations that simulated neutralized and acidic
328 PLA degradation products, we similarly observed bioenergetic alterations, excluding pH as a confounder.
329 Lastly, using aminooxyacetic acid to modulate some adverse responses to PLA degradation products,
330 suggests that acidity is not solely the driver of immune cellular activation to PLA.
331 Our findings using sterile implants present a perspective different than what is observed with
332 bacterial endotoxin (LPS). Within 1h of exposure to very low endotoxin concentrations, significant metabolic
333 changes characterized by increased glycolysis and decreased oxidative phosphorylation occurs[35]; with PLA
334 degradation products, we only observed changes after several days of exposure, with distinct metabolism.
335 Importantly, LPS decreases ATP levels[35,55]; in contrast, PLA degradation products (including monomeric L-
336 lactic acid) increase ATP levels as shown in this study. Lastly, unlike PLA degradation products, LPS-
337 mediated glycolytic reprogramming is reliant on IL-1β signaling[36].
338 Lactate is a signaling molecule in immunity[56] and cancer progression[57-59]. Its role when combined
339 with LPS is conflicting, with reports of proinflammatory and anti-inflammatory effects[60,61]. However, a stand-
340 alone ability of lactate to activate immune cells is novel, as prior inflammatory and cancer models did not
341 simulate prolonged exposure times, a critical feature of the cancer and immune microenvironments.
342 Amorphous PLA which undergoes faster hydrolytic degradation than crystalline PLA results in
343 quicker onset of metabolic reprogramming. Nonetheless, crystalline PLA does eventually result in metabolic
344 remodeling and altered bioenergetics. Furthermore, our data implicate monocarboxylate transporters which
345 mediate the bi-directional flux of lactate across cell membranes[33,60].
346 Glucose is the first substrate in glycolysis. As such, radiolabeled glucose (FDG) uptake is often
347 used to measure glycolytic dependence, in-vivo, such as in some cancers or inflammatory disorders where
348 enhanced glycolysis is pivotal to disease progression[62]. We observed increased glycolytic dependence in
349 the PLA inflammatory microenvironment using sterile amorphous PLA, which was abrogated by 2DG, one
350 of the glycolytic inhibitors applied in our in-vitro studies. Unsurprisingly, after surgical resection of colorectal
351 and cervical tumors in human patients, chronic, sterile inflammation from PLA-based adhesion barriers
352 elevate FDG uptake, falsely mimicking cancer recurrence[63,64].
353 Surprisingly, 2DG did not significantly reduce macrophage recruitment as measured by expression
354 of CD11b or F4/80 in the PLA microenvironment. However, 2DG reduced macrophage activation into a
355 proinflammatory phenotype (CD86), likely by competing with radiolabeled glucose for binding to
356 hexokinase[36], thereby inhibiting the first step in glycolysis. Since hydroxyapatite (HA) is often used to
357 neutralize acidity from PLA degradation[10], we compared effects of incorporating similar amounts (w/w) of
358 HA to 2DG toward clinical translation of techniques targeting metabolism. Compared to 2DG, we observed
359 increased pro-regenerative macrophage expression (CD206) with HA, which is consistent with the
360 bioactivity of ceramic biomaterials[44], opening the possibility of combinatorial strategies for regenerative
361 applications. Corroborating CD206 results, our in-vitro data showed that neither 2DG nor 3PO, as a
362 glycolytic inhibitor for PLA-based application, increases IL-4 or IL-10.
363 Compared to inhibiting glycolysis using 2DG, neutralizing acidity using HA increased macrophage
364 recruitment and proinflammatory polarization, suggesting that metabolism and not acidity, is at the center
365 of adverse immune responses to bulk PLA implants and PLA degradation products. Contrary to some
366 studies, an explanation for the inability of HA to reduce inflammation in our study could be the amount used.
367 Whereas the w/w concentration of HA present in our fabricated composites was 2 % for direct comparison
368 to 2DG, greater than 20 % HA concentrations are more often used[65,66]. However, it is noteworthy that 2%
369 HA resulted in significantly increased CD206 expression, suggesting pharmacological efficacy, yet could
370 not reduce CD86 expression. Furthermore, unlike in soft tissue regeneration, enhanced mechanical
371 properties of implants having more concentration of or comprising of only HA is desirable for bone tissue
372 engineering[65,66].

373   Increased fibroblast activation, measured by α-SMA expression, in the PLA microenvironment was
374   reduced by inhibiting glycolysis using 2DG and not neutralizing acidity using HA. Compared to HA, 2DG
375   reduced both α-SMA and TGF-β expression, suggesting that underlying metabolism regulates fibroblast
376   activation in the PLA microenvironment. In agreement, metabolic reprogramming is known to play a key
377   role in profibrotic disorders, activating fibroblasts[19].
378   Most, if not all, publications on PLA's biomedical application include a statement indicating that
379   PLA breakdown products are metabolized through the tricarboxylic acid cycle. However, not until this study
380   has it been demonstrated that bioenergetic changes occur in response to PLA. This key observation will
381   redirect the field of tissue engineering, by offering an opportunity to intervene in this response. It opens up
382   the possibilities to computationally identify relevant small molecules that could be clinically deployed,
383   embedded in PLA implants, to mitigate adverse responses after carefully tuning drug release profiles.
384   Moreover, use of PLA composites with ceramics could be optimized by combining the benefits of metabolic
385   reprogramming with bioactivity of ceramics for bone tissue engineering. Beyond its ability to inhibit uptake
386   of glycolytic substrates, related glutamine metabolic pathways, affected by aminooxyacetic acid could be
387   explored for driving pro-regenerative macrophage response[67].
388   Taken together, our findings suggest a model where PLA degradation products, including
389   monomers of L-lactic acid, mechanistically remodel metabolism in cells of the immune microenvironment.
390   This mechanism is specific and leads to increased proinflammatory cytokine and marker expression which
391   can be modulated while stimulating anti-inflammatory cytokines. Our approach will enhance the
392   biocompatibility and safety of biomaterials, including PLA-based implants for soft- and hard-tissue
393   regeneration, significantly advancing tissue engineering.
394

395   **Methods**
396   **Polylactide (PLA) materials and extraction.** Highly crystalline PLA 3100HP and amorphous PLA 4060D
397   (both from NatureWorks LLC) were used after their physicochemical and thermal properties were
398   authenticated (Supplementary Table 1). PLA was sterilized by exposure to ultraviolet radiation for 30
399   minutes[25]. Afterwards, breakdown products (extracts)[21] of PLA were obtained by suspending 4 g of PLA
400   pellets in 25 ml of complete medium. Complete medium comprised of DMEM medium, 10% heat-inactivated
401   Fetal Bovine Serum and 100 U/mL penicillin-streptomycin (all from ThermoFisher Scientific). PLA was
402   extracted for 12 days in an orbital shaker at 250 rpm and 37 °C, after which extracts were decanted and
403   extract's pH measured. Either 100 or 150 μl of extract (specified in each figure legend) was used per well
404   of a flat-bottom 96-well plate; each volume was made up to 200 μl, as final volume, using freshly made
405   complete medium.
406

407   **Bioenergetic assessment.** Bioluminescence was measured using the IVIS Spectrum in vivo imaging
408   system (PerkinElmer) after adding 150 μg/mL of D-luciferin (PerkinElmer). Living Image (Version 4.5.2,
409   PerkinElmer) was used for acquiring bioluminescence on the IVIS Spectrum. Standard ATP/ADP kits
410   (Sigma-Aldrich) containing D-luciferin, luciferase and cell lysis buffer were used to according to
411   manufacturer's instructions. Luminescence at integration time of 1000 ms was obtained using the
412   SpectraMax M3 Spectrophotometer (Molecular Devices) using SoftMax Pro (Version 7.0.2, Molecular
413   Devices).
414

415   **pH measurements**. The pH of extracts was assessed using an Orion Star A111 Benchtop pH Meter
416   (ThermoFisher Scientific) under room temperature conditions (20 °C).
417

418   **Microscopy.** Z-stack microscopy was accomplished by using the DeltaVision deconvolution imaging
419   system (GE Healthcare) and softWoRx software (Version 7.2.1, GE Healthcare) at excitation and emission
420   wavelengths of 525 and 558 nm, respectively for FITC. Section thickness of 0.2 μm for 64 to 128 sections
421   were obtained at 40x and 100x magnification while imaging. Chambered Coverglass (Nunc Lab-Tek II) was
422   used to seed 20,000 BGL cells (see cells below), keeping similar ratios as in a 96-well plate for volume of
423   PLA extracts to volume of fresh medium.
424

Glucose measurement. Glucose levels in complete medium was evaluated by a hand-held GM-100 glucose meter (BioReactor Sciences) after validation (Supplementary Fig. 1b) according to manufacturer's instruction.

Cells. Mouse embryonic fibroblast cell line (NIH 3T3 cell line; ATCC) and murine primary bone-marrow derived macrophages (BMDMs) were used. In each experiment, either 5,000 fibroblasts or 50,000 BMDMs were initially seeded. BMDMs were sourced from male and female C57BL/6J mice (Jackson Laboratories) of 3-4 months[30,35]. NIH 3T3 cells were stably transfected with a Sleeping Beauty transposon plasmid (pLuBIG) having a bidirectional promoter driving an improved firefly luciferase gene (fLuc) and a fusion gene encoding a Blasticidin-resistance marker (BsdR) linked to eGFP (BGL)[26]; enabling us to simultaneously monitor morphological and bioenergetic changes in live cells[68,69]. All cells were cultured in a total of 200 μl complete medium with volumes of extracts specified in figure legends.

Materials. 3-(3-pyridinyl)-1-(4-pyridinyl)-2-propen-1-one (MilliporeSigma), 2-deoxyglucose (MilliporeSigma) and aminooxyacetic acid (Sigma-Aldrich) were used for glycolytic inhibition and L-lactic acid (Sigma-Aldrich) was used at various concentrations to reproduce the effects of PLA degradation products. Each of these materials were made in complete medium before adding to wells of a 96-well plate.

Cell viability. Cell viability was assessed using the crystal violet staining assay[29], at room temperature, as an end-point measure of total biomass generated over the course of the culture period. Briefly, out of 200 μl of medium per well, 150 μl is discarded. To each well, 150 μl of 99.9 % methanol (MilliporeSigma) is added for 15 mins to kill and fix the cells, then discarded. Afterwards, 100 μl of 0.5 % crystal violet (25 % methanol) is added for 20 mins, then the wells are emptied. Each well is washed twice with 200 μl of phosphate buffered saline for 2 mins. Absorbance (optical density) was acquired at 570 nm using the the SpectraMax M3 Spectrophotometer (Molecular Devices) and SoftMax Pro software (Version 7.0.2, Molecular Devices).

Functional metabolism. Basal measurements of oxygen consumption rate (OCR), extracellular acidification rate (ECAR) and lactate-linked proton efflux rate (PER) were obtained in real-time using the Seahorse XFe-96 Extracellular Flux Analyzer (Agilent Technologies)[34-36]. Prior to running the assay, cell culture medium was washed with and replaced by the Seahorse XF DMEM medium (pH 7.4) supplemented with 25 mM D-glucose and 4 mM Glutamine. The Seahorse plates were equilibrated in a non-CO_2 incubator for an hour prior to the assay. The Seahorse ATP rate and cell energy phenotype assays were run according to manufacturer's instruction and all reagents for the Seahorse assays were sourced from Agilent Technologies. Wave software (Version 2.6.1) was used to export Seahorse data directly as means ± standard deviation (SD).

Chemokine and cytokine measurements. Cytokine and chemokine levels were measured using a MILLIPLEX MAP mouse magnetic bead multiplex kit (MilliporeSigma)[39] to assess for IL-6, MCP-1, TNF-α, IL-1β, IL-4, IL-10, IFN-λ and 1L-13 protein expression in supernatants. Data was acquired using Luminex 200 (Luminex Corporation) by the xPONENT software (Version 3.1, Luminex Corporation). Using the glycolytic inhibitor, 3PO, expectedly decreased cytokine values to < 3.2 pg/ mL in some experiments. For statistical analyses, those values were expressed as 3.1 pg/ mL. Values exceeding the dynamic range of the assay, in accordance with manufacturer's instruction, were excluded. Additionally, IL-6 ELISA kits (RayBiotech) for supernatants were used according to manufacturer's instructions.

D/L-lactic acid determination assays. Measurements of L- and D-lactic acid were using standard D- and L-lactate assay kits (Sigma-Aldrich) according to manufacturer's instruction after optimization (Supplementary Fig. 5a-b). Negative absorbance values which were outside the dynamic range for the assay were excluded during analysis.

Optical rotation. Polarimetry was used to characterize the L-content and optical purity of the PLA samples with a P-2000 polarimeter (Jasco) by the Spectra Manager software (Version 2.13.00, Jasco). The optical

15

478 rotation, $[\alpha]_{25}$, was measured and averaged for three samples of each polymer in chloroform (Omnisolv), at
479 a concentration of 1 g/ mL. Conditions were set at 25 ºC and 589 nm wavelength. Sucrose was used as a
480 standard reference material, and its specific optical rotation was reported as approximately 67 º.
481
482 **Gel permeation chromatography.** Gel permeation chromatography (GPC) was conducted to characterize
483 the polymer molecular weights using a 600 controller (Waters) equipped with Optilab T-rEX refractive index
484 (RI) and TREOS II multi-angle light scattering (MALS) detectors (Wyatt Technology Corporation), and a
485 PLgel 5μm MIXED-C column (Agilent Technologies) with chloroform eluent (1 mL/min). ASTRA software
486 (Version 7.3.2.21, Wyatt Technology Corporation) was used. Polystyrene standards (Alfa Aesar) with M_n
487 ranging from 35,000 to 900,000 Da were used for calibration.
488
489 **Differential scanning calorimetry.** Differential scanning calorimetry (DSC) was conducted with a DSC
490 Q20 (TA Instruments) to analyse the melting temperature (T_m), glass transition temperature (T_g), and
491 percent crystallinity of the PLA grades. Thermal Advantage software (Version 5.5.23, TA Instruments) was
492 used. Temperature was first equilibrated to 0 ºC, then ramped up to 200 ºC at a heating rate of 10 ºC/ min;
493 temperature was then held isothermally for 5 minutes. Afterwards, the sample was cooled back to 0 ºC at
494 a rate of 10 ºC/min, then held isothermally for 2 minutes. Finally, the material was heated back to 200 ºC
495 at 10 ºC/ min.
496
497 **In-vivo studies, tissue processing and analyses.** Amorphous PLA was compounded with 2DG at 190
498 ºC for 3 mins in a DSM 15 cc mini-extruder (DSM Xplore) and pelletizer (Leistritz Extrusion Technology).
499 Our in-vitro studies indicate 1 mM 2DG to be an effective concentration. Accordingly, we estimated that 189
500 mg of 2DG in 10 g of amorphous PLA will approximate effective concentrations after accounting for potential
501 thermal degradation of 2DG, converting mM to w/ w values[70]. We compounded comparable amounts (200
502 mg) of hydroxyapatite (HA; 2.5 μm^2 particle sizes[42]; Sigma-Aldrich) in 10 g of amorphous PLA under the
503 same melt-blending thermal conditions. To exclude the effect of melt-blending as a confounder in our
504 studies, amorphous PLA controls were processed under the same thermal conditions to make
505 "reprocessed" amorphous PLA. Pellets from melt-blending were made into 1.75 mm diameter filaments
506 using an extruder (Filabot EX2) at 170 ºC with air set at 93. For surgical implantation, amorphous PLA
507 filaments were cut into 1 mm lengths; four biomaterials were subcutaneously implanted on the dorsum
508 (back) of each mouse, with two cranially (2.5 cm apart) and two caudally (2.5 cm apart)[12].
509
510 Two-month old female C57BL/6J mice (n = 3 mice per group) with an average weight of 19 g were used
511 according to procedures approved by the Institutional Animal Care and Use Committee at Michigan State
512 University (PROTO202100327). Mice were anesthetized using isoflurane (2-3 %). The back of each mouse
513 was shaved and alternate iodine and alcohol swabs were used as skin disinfectants. Aseptic surgery
514 consisted of incisions through the skin into the subcutis, where biomaterials were inserted into a pouch
515 made with forceps. Afterwards, surgical glue (3M Vetbond) was used to appose the skin. Each mouse
516 received intraperitoneal or subcutaneous pre- and post-operative meloxicam (5 mg/ kg) injections as well
517 as postoperative saline. Sham controls underwent the same procedure without biomaterial implantation.
518 After 6 weeks, the dorsum of mice was shaved to visibly observe sites of surgical implantation. Thereafter,
519 mice were intraperitoneally injected with 4.82 MBq F-18 fluorodeoxyglucose (Cardinal Health) in 200 μl. At
520 65 mins post-dose, mice were euthanized and blood drawn from their hearts. Circular biopsies (12 mm
521 diameter) of full skin thickness, with visible implants in the center, were recovered. Similar sized biopsies
522 were collected from mice in the sham group in the region where surgical incision was made. Biomaterial
523 migration from subcutaneous sites only allowed for the recovery of most and not all implants. As such, for
524 obtaining data on the gamma counter (Fig. 7a), there were 12 skin biopsies from 3 mice in the sham group,
525 8 skin biopsies from 3 mice (amorphous PLA group) and 10 skin biopsies from 3 mice (amorphous + 2DG
526 group). Skin biopsies, blood sample and heart organs were weighed, with only skin samples fixed in 4%
527 paraformaldehyde (PFA). Activity in all samples was assessed via gamma counter (Wizard 2, Perkin Elmer)
528 once decayed to a linear range. All injected doses and gamma counter measurements were decay-
529 corrected to the same timepoint to calculate the percent of injected dose taken up per gram of assessed
530 tissue (% ID / g; Fig. 7a).

16

531
532   For tissue staining, one skin biopsy per mouse was passed through increasing concentration of 10 %, 20
533   % and 30 % sucrose, daily. Using 99.9% methanol (Sigma-Aldrich) on dry ice, tissues were embedded in
534   optimal cutting temperature (O.C.T.) compound (Tissue-Tek) by snap freezing. After equilibration at -20 ºC,
535   multiple successive 8 μm sections were obtained using a microtome-cryostat. Sections were routinely
536   stained using hematoxylin and eosin. Two different tissue sections were immunostained using conjugated
537   antibodies as follows: 1) F4/80-FITC (1:100; BioLegend; 123107), CD11b-PE (1:100; BioLegend; 101207),
538   CD206-BV421 (1:200; BioLegend; 141717) and CD86-Alexa Fluor 647 (1:100; BioLegend; 105019) using
539   ordinary mounting medium; 2) alpha-SMA-eFluor660 (1:150; ThermoFisher Scientific; 50-9760-82), TGF-
540   beta-PE (1:100; ThermoFisher Scientific; 12-9821-82) using DAPI mounting medium. Sections for TGF-
541   beta were permeabilized using 0.1% Triton X in 1x PBS (PBST) for 8 mins then washed off with 1x PBS
542   generously. Afterwards, blocking buffer (0.5 % bovine serum albumin in 1x PBS) was used to cover slides
543   for 30 mins. Slides were then incubated in antibodies at 4 °C overnight. Subsequently, slides with tissue
544   sections were washed in 1x PBS, and mounting medium applied.
545
546   Immunostained sections on slides were imaged using a Leica DMi8 Thunder microscope fitted with a
547   DFC9000 GTC sCMOS camera and LAS-X software (Leica, version 3.7.4). Imaging settings at 20x
548   magnification and 100 % intensity were: 1) F4/80-FITC excitation using the 475 laser (filter 535/ 70; 500
549   ms); CD11b-PE excitation using the 555 laser (no filter; 500 ms); CD206-BV421 excitation using 395 laser
550   (no filter; 150 ms); CD86-Alexa Fluor 647 excitation using the 635 laser (no filter; 500 ms). 2) alpha-SMA-
551   eFluor660 excitation using the 635 laser (no filter; 500 ms), TGF-beta-PE excitation using the 555 laser (no
552   filter; 500 ms) and DAPI excitation using the 395 laser (535 filter; 500 ms). On the other hand, sections
553   stained with hematoxylin and eosin were imaged at 40x using the Nikon Eclipse Ci microscope fitted with
554   a CoolSNAP DYNO (Photometrics) and NIS elements BR 5.21.02 software (Nikon Instruments Inc.).
555   Microscope images were prepared and analyzed using ImageJ (version 1.53k). For analyzing
556   immunostained sections, 5 randomly selected rectangular areas of interest (1644.708 μm^2), encompassing
557   cells adjacent to implants, were obtained as mean gray values[71] a tissue section. In the sham group,
558   biopsies were taken from incision sites and areas without cells were also analyzed. Where derived from n
559   = 2 or n = 3 mice, 10 or 15 data points, respectively are graphically represented to fully reveal inherent
560   variance across samples (Fig. 7b-e; Fig. 8a-b); only the aPLA + HA group had sections derived from n = 2
561   mice after one sample was damaged during cryo-sectioning and excluded from analyses. Representative
562   images (16-bit; 0 to 65,535) were adjusted to enhance contrast for direct comparison using ImageJ as
563   follows: CD86 (800 – 11,000), CD206 (2,000 – 5,000), F4/80 (500 – 4,000), CD11b (800 – 11,000), SMA
564   (1,300 – 5,000), DAPI (6,000 – 31, 000), TGF (1,900 – 13,000).
565
566   **Statistics and reproducibility.** Statistical software (GraphPad Prism) was used to analyse data presented
567   as mean with standard deviation (SD). Significance level was set at $p < 0.05$, and details of statistical tests
568   and sample sizes, which are biological replicates, are provided in figure legends. Exported data (mean, SD)
569   from Wave in Seahorse experiments had the underlying assumption of normality and similar variance, and
570   thus were tested using corresponding parametric tests as indicated in figure legends.
571
572   **Data availability.** The data supporting the findings of this study are available within the paper and its
573   Supplementary Information.
574
575   **References**
576   1   Farah, S., Anderson, D. G. & Langer, R. Physical and mechanical properties of PLA, and
577   their functions in widespread applications - A comprehensive review. *Adv Drug Deliv Rev*
578   **107**, 367-392, doi:10.1016/j.addr.2016.06.012 (2016).
579   2   Givissis, P. K., Stavridis, S. I., Papagelopoulos, P. J., Antonarakos, P. D. & Christodoulou, A.
580   G. Delayed foreign-body reaction to absorbable implants in metacarpal fracture
581   treatment. *Clinical Orthopaedics and Related Research®* **468**, 3377-3383 (2010).

3   Laine, P., Kontio, R., Lindqvist, C. & Suuronen, R. Are there any complications with bioabsorbable fixation devices?: a 10 year review in orthognathic surgery. *International journal of oral and maxillofacial surgery* **33**, 240-244 (2004).

4   Chalidis, B., Kitridis, D., Savvidis, P., Papalois, A. & Givissis, P. Does the Inion OTPStm absorbable plating system induce higher foreign-body reaction than titanium implants? An experimental randomized comparative study in rabbits. *Biomedical Materials* **15**, 065011 (2020).

5   Poh, P. S. *et al.* Polylactides in additive biomanufacturing. *Advanced Drug Delivery Reviews* **107**, 228-246 (2016).

6   Ramot, Y., Haim-Zada, M., Domb, A. J. & Nyska, A. Biocompatibility and safety of PLA and its copolymers. *Adv Drug Deliv Rev* **107**, 153-162, doi:10.1016/j.addr.2016.03.012 (2016).

7   Mosier-LaClair, S., Pike, H. & Pomeroy, G. Intraosseous bioabsorbable poly-L-lactic acid screw presenting as a late foreign-body reaction: a case report. *Foot & ankle international* **22**, 247-251 (2001).

8   Athanasiou, K. A., Agrawal, C. M., Barber, F. A. & Burkhart, S. S. Orthopaedic applications for PLA-PGA biodegradable polymers. *Arthroscopy* **14**, 726-737, doi:10.1016/s0749-8063(98)70099-4 (1998).

9   Waris, E. *et al.* Long-term bone tissue reaction to polyethylene oxide/polybutylene terephthalate copolymer (Polyactive®) in metacarpophalangeal joint reconstruction. *Biomaterials* **29**, 2509-2515 (2008).

10   Agrawal, C. M. & Athanasiou, K. A. Technique to control pH in vicinity of biodegrading PLA-PGA implants. *J Biomed Mater Res* **38**, 105-114, doi:10.1002/(sici)1097-4636(199722)38:2<105::aid-jbm4>3.0.co;2-u (1997).

11   Taylor, M. S., Daniels, A. U., Andriano, K. P. & Heller, J. Six bioabsorbable polymers: in vitro acute toxicity of accumulated degradation products. *J Appl Biomater* **5**, 151-157, doi:10.1002/jab.770050208 (1994).

12   Deng, M. *et al.* Dipeptide-based Polyphosphazene and Polyester Blends for Bone Tissue Engineering. *Biomaterials* **31**, 4898-4908, doi:10.1016/j.biomaterials.2010.02.058 (2010).

13   Pajares-Chamorro, N. *et al.* Silver-doped bioactive glass particles for in vivo bone tissue regeneration and enhanced methicillin-resistant Staphylococcus aureus (MRSA) inhibition. *Materials Science and Engineering: C* **120**, 111693 (2021).

14   Lih, E. *et al.* A Bioinspired Scaffold with Anti-Inflammatory Magnesium Hydroxide and Decellularized Extracellular Matrix for Renal Tissue Regeneration. *ACS Cent Sci* **5**, 458-467, doi:10.1021/acscentsci.8b00812 (2019).

15   Xu, T. O., Kim, H. S., Stahl, T. & Nukavarapu, S. P. Self-neutralizing PLGA/magnesium composites as novel biomaterials for tissue engineering. *Biomed Mater* **13**, 035013, doi:10.1088/1748-605X/aaaa29 (2018).

16   Kamata, M., Sakamoto, Y. & Kishi, K. Foreign-body reaction to bioabsorbable plate and screw in craniofacial surgery. *Journal of Craniofacial Surgery* **30**, e34-e36 (2019).

17   Narayanan, G., Vernekar, V. N., Kuyinu, E. L. & Laurencin, C. T. Poly (lactic acid)-based biomaterials for orthopaedic regenerative engineering. *Advanced drug delivery reviews* **107**, 247-276 (2016).

624 18   Gonzalez-Lomas, G., Cassilly, R. T., Remotti, F. & Levine, W. N. Is the etiology of pretibial
625   cyst formation after absorbable interference screw use related to a foreign body
626   reaction? *Clinical Orthopaedics and Related Research®* **469**, 1082-1088 (2011).
627 19   Xie, N. *et al.* Glycolytic reprogramming in myofibroblast differentiation and lung fibrosis.
628   *American journal of respiratory and critical care medicine* **192**, 1462-1474 (2015).
629 20   O'Neill, L. A. & Pearce, E. J. in *J Exp Med* Vol. 213   15-23 (2016).
630 21   Ignatius, A. A. & Claes, L. E. In vitro biocompatibility of bioresorbable polymers: poly(L,
631   DL-lactide) and poly(L-lactide-co-glycolide). *Biomaterials* **17**, 831-839, doi:10.1016/0142-
632   9612(96)81421-9 (1996).
633 22   Yang, Y. *et al.* In vitro degradation of porous poly (l-lactide-co-glycolide)/β-tricalcium
634   phosphate (PLGA/β-TCP) scaffolds under dynamic and static conditions. *Polymer
635   Degradation and Stability* **93**, 1838-1845 (2008).
636 23   Bostman, O. M. & Pihlajamaki, H. K. Adverse tissue reactions to bioabsorbable fixation
637   devices. *Clin Orthop Relat Res*, 216-227 (2000).
638 24   Choueka, J. *et al.* Canine bone response to tyrosine-derived polycarbonates and poly(L-
639   lactic acid). *J Biomed Mater Res* **31**, 35-41, doi:10.1002/(sici)1097-
640   4636(199605)31:1<35::aid-jbm5>3.0.co;2-r (1996).
641 25   Athanasiou, K. A., Niederauer, G. G. & Agrawal, C. M. Sterilization, toxicity,
642   biocompatibility and clinical applications of polylactic acid/polyglycolic acid copolymers.
643   *Biomaterials* **17**, 93-102, doi:10.1016/0142-9612(96)85754-1 (1996).
644 26   Kanada, M. *et al.* Differential fates of biomolecules delivered to target cells via
645   extracellular vesicles. *Proceedings of the National Academy of Sciences* **112**, E1433-E1442
646   (2015).
647 27   Frottin, F. *et al.* The nucleolus functions as a phase-separated protein quality control
648   compartment. *Science* **365**, 342-347 (2019).
649 28   Hui, S. *et al.* Glucose feeds the TCA cycle via circulating lactate. *Nature* **551**, 115-118
650   (2017).
651 29   Feoktistova, M., Geserick, P. & Leverkus, M. Crystal violet assay for determining viability
652   of cultured cells. *Cold Spring Harbor Protocols* **2016**, pdb. prot087379 (2016).
653 30   Gonçalves, R. & Mosser, D. M. The isolation and characterization of murine macrophages.
654   *Current protocols in immunology* **111**, 14.11. 11-14.11. 16 (2015).
655 31   Infantino, V., Iacobazzi, V., Palmieri, F. & Menga, A. ATP-citrate lyase is essential for
656   macrophage inflammatory response. *Biochemical and biophysical research
657   communications* **440**, 105-111 (2013).
658 32   Jijon, H. B. *et al.* Inhibition of poly (ADP-ribose) polymerase attenuates inflammation in a
659   model of chronic colitis. *American Journal of Physiology-Gastrointestinal and Liver
660   Physiology* **279**, G641-G651 (2000).
661 33   Tan, Z. *et al.* in *The Journal of biological chemistry* Vol. 290   46-55 (2015).
662 34   Ip, W. E., Hoshi, N., Shouval, D. S., Snapper, S. & Medzhitov, R. Anti-inflammatory effect
663   of IL-10 mediated by metabolic reprogramming of macrophages. *Science* **356**, 513-519
664   (2017).
665 35   Mills, E. L. *et al.* Succinate Dehydrogenase Supports Metabolic Repurposing of
666   Mitochondria to Drive Inflammatory Macrophages. *Cell* **167**, 457-470.e413,
667   doi:10.1016/j.cell.2016.08.064 (2016).

668 36 Tannahill, G. *et al.* Succinate is a danger signal that induces IL-1β via HIF-1α. *Nature* **496**,
669   238-242, doi:10.1038/nature11986 (2013).
670 37 Clem, B. *et al.* Small-molecule inhibition of 6-phosphofructo-2-kinase activity suppresses
671   glycolytic flux and tumor growth. *Molecular cancer therapeutics* **7**, 110-120 (2008).
672 38 Kauppinen, R. A., Sihra, T. S. & Nicholls, D. G. Aminooxyacetic acid inhibits the malate-
673   aspartate shuttle in isolated nerve terminals and prevents the mitochondria from utilizing
674   glycolytic substrates. *Biochim Biophys Acta* **930**, 173-178, doi:10.1016/0167-
675   4889(87)90029-2 (1987).
676 39 Sprague, L. *et al.* Dendritic cells: in vitro culture in two-and three-dimensional collagen
677   systems and expression of collagen receptors in tumors and atherosclerotic
678   microenvironments. *Experimental cell research* **323**, 7-27 (2014).
679 40 Philpott, G. W. *et al.* RadioimmunoPET: detection of colorectal carcinoma with positron-
680   emitting copper-64-labeled monoclonal antibody. *Journal of Nuclear Medicine* **36**, 1818-
681   1824 (1995).
682 41 Wen, S.-S. *et al.* Metabolic reprogramming and its clinical application in thyroid cancer.
683   *Oncology Letters* **18**, 1579-1584 (2019).
684 42 Pérez, E. Mechanical performance of in vitro degraded polylactic acid/hydroxyapatite
685   composites. *Journal of Materials Science* **56**, 19915-19935 (2021).
686 43 Graney, P. L., Lurier, E. B. & Spiller, K. L. Biomaterials and bioactive factor delivery systems
687   for the control of macrophage activation in regenerative medicine. *ACS Biomaterials
688   Science & Engineering* **4**, 1137-1148 (2017).
689 44 Xue, H. *et al.* Enhanced tissue regeneration through immunomodulation of angiogenesis
690   and osteogenesis with a multifaceted nanohybrid modified bioactive scaffold. *Bioactive
691   Materials* (2022).
692 45 Veiseh, O. *et al.* Size- and shape-dependent foreign body immune response to materials
693   implanted in rodents and non-human primates. *Nat Mater* **14**, 643-651,
694   doi:10.1038/nmat4290 (2015).
695 46 Pariente, J.-L., Kim, B.-S. & Atala, A. In vitro biocompatibility evaluation of naturally
696   derived and synthetic biomaterials using normal human bladder smooth muscle cells. *The
697   Journal of urology* **167**, 1867-1871 (2002).
698 47 Andersson, S. R., Hakkarainen, M., Inkinen, S., Södergård, A. & Albertsson, A.-C.
699   Polylactide stereocomplexation leads to higher hydrolytic stability but more acidic
700   hydrolysis product pattern. *Biomacromolecules* **11**, 1067-1073 (2010).
701 48 Kozlov, A. M., Lone, A., Betts, D. H. & Cumming, R. C. Lactate preconditioning promotes a
702   HIF-1α-mediated metabolic shift from OXPHOS to glycolysis in normal human diploid
703   fibroblasts. *Scientific reports* **10**, 1-16 (2020).
704 49 Olive, A. J., Kiritsy, M. & Sassetti, C.   (Am Assoc Immnol, 2021).
705 50 Iliopoulos, D., Hirsch, H. A. & Struhl, K. An epigenetic switch involving NF-κB, Lin28, Let-7
706   MicroRNA, and IL6 links inflammation to cell transformation. *Cell* **139**, 693-706 (2009).
707 51 Eming, S. A., Wynn, T. A. & Martin, P. Inflammation and metabolism in tissue repair and
708   regeneration. *Science* **356**, 1026-1030 (2017).
709 52 Jiang, W. & Xu, J. Immune modulation by mesenchymal stem cells. *Cell proliferation* **53**,
710   e12712 (2020).

53   Pajarinen, J. *et al.* Mesenchymal stem cell-macrophage crosstalk and bone healing. *Biomaterials* **196**, 80-89 (2019).

54   Swartzlander, M. D. *et al.* Immunomodulation by mesenchymal stem cells combats the foreign body response to cell-laden synthetic hydrogels. *Biomaterials* **41**, 79-88 (2015).

55   Van den Bossche, J. *et al.* Mitochondrial dysfunction prevents repolarization of inflammatory macrophages. *Cell reports* **17**, 684-696 (2016).

56   Manoharan, I., Prasad, P. D., Thangaraju, M. & Manicassamy, S. Lactate-Dependent Regulation of Immune Responses by Dendritic Cells and Macrophages. *Frontiers in Immunology*, 3062 (2021).

57   Zhang, A. *et al.* Lactate-induced M2 polarization of tumor-associated macrophages promotes the invasion of pituitary adenoma by secreting CCL17. *Theranostics* **11**, 3839 (2021).

58   Lin, S. *et al.* Lactate-activated macrophages induced aerobic glycolysis and epithelial-mesenchymal transition in breast cancer by regulation of CCL5-CCR5 axis: a positive metabolic feedback loop. *Oncotarget* **8**, 110426 (2017).

59   Romero-Garcia, S., Moreno-Altamirano, M. M. B., Prado-Garcia, H. & Sánchez-García, F. J. Lactate contribution to the tumor microenvironment: mechanisms, effects on immune cells and therapeutic relevance. *Frontiers in immunology* **7**, 52 (2016).

60   Samuvel, D. J., Sundararaj, K. P., Nareika, A., Lopes-Virella, M. F. & Huang, Y. Lactate boosts TLR4 signaling and NF-κB pathway-mediated gene transcription in macrophages via monocarboxylate transporters and MD-2 up-regulation. *The Journal of Immunology* **182**, 2476-2484 (2009).

61   Yang, K. *et al.* Lactate Suppresses Macrophage Pro-Inflammatory Response to LPS Stimulation by Inhibition of YAP and NF-κB Activation via GPR81-Mediated Signaling. *Frontiers in Immunology* **11**, 2610 (2020).

62   Tang, C.-Y. & Mauro, C. Similarities in the metabolic reprogramming of immune system and endothelium. *Frontiers in immunology* **8**, 837 (2017).

63   Hsieh, T.-C. & Hsu, C.-W. Foreign body reaction mimicking local recurrence from polyactide adhesion barrier film after laparoscopic colorectal cancer surgery: A retrospective cohort study. *Medicine* **101** (2022).

64   Chong, G. O., Lee, Y. H., Hong, D. G., Cho, Y. L. & Lee, Y. S. Unabsorbed polylactide adhesion barrier mimicking recurrence of gynecologic malignant diseases with increased 18F-FDG uptake on PET/CT. *Archives of Gynecology and Obstetrics* **292**, 191-195 (2015).

65   Bernardo, M. P. *et al.* PLA/Hydroxyapatite scaffolds exhibit in vitro immunological inertness and promote robust osteogenic differentiation of human mesenchymal stem cells without osteogenic stimuli. *Scientific reports* **12**, 1-15 (2022).

66   Kim, S.-S., Park, M. S., Jeon, O., Choi, C. Y. & Kim, B.-S. Poly (lactide-co-glycolide)/hydroxyapatite composite scaffolds for bone tissue engineering. *Biomaterials* **27**, 1399-1409 (2006).

67   Jha, A. K. *et al.* Network integration of parallel metabolic and transcriptional data reveals metabolic modules that regulate macrophage polarization. *Immunity* **42**, 419-430, doi:10.1016/j.immuni.2015.02.005 (2015).

753 68   Kanada, M. *et al.* Microvesicle-mediated delivery of minicircle DNA results in effective gene-directed enzyme prodrug cancer therapy. *Molecular cancer therapeutics* **18**, 2331-2342 (2019).

756 69   Negrin, R. S. & Contag, C. H. In vivo imaging using bioluminescence: a tool for probing graft-versus-host disease. *Nature Reviews Immunology* **6**, 484-490 (2006).

758 70   Poon, C. Measuring the density and viscosity of culture media for optimized computational fluid dynamics analysis of in vitro devices. *Journal of the Mechanical Behavior of Biomedical Materials* **126**, 105024 (2022).

761 71   Bravo-Hernandez, M. *et al.* Spinal subpial delivery of AAV9 enables widespread gene silencing and blocks motoneuron degeneration in ALS. *Nature medicine* **26**, 118-130 (2020).

769 **Author contributions.** Conceptualization, C.V.M. and C.H.C.; Methodology, C.V.M., K.R.Z., K.D.H., S.B.G., R.N. and C.H.C.; Investigation, C.V.M., M.A., E.U., M.O.B., M.M.K., K.S., A.V.M., H.P., S.C., J.M.H C.L.M., S.J.C., M.H. and A.T.; Writing – Original Draft, C.V.M.; Writing – Review & Editing, C.V.M., M.A., E.U., M.O.B., M.M.K., K.S., A.V.M., H.P., S.C., J.M.H C.L.M., S.J.C., M.H., A.T., K.R.Z., K.D.H., S.B.G., R.N. and C.H.C.; Funding Acquisition, C.H.C.; Resources, R.N. and C.H.C.; Supervision, K.R.Z., K.D.H., S.B.G., R.N. and C.H.C.

776 **Competing interests.** C.V.M and C.H.C are inventors on a pending patent application filed by Michigan State University on metabolic reprogramming to biodegradable polymers.